Optics Communications 437 (2019) 148–152

Contents lists available at ScienceDirect

Optics Communications

journal homepage: www.elsevier.com/locate/optcom

Fringe pattern denoising based on deep learning

Ketao Yan [a], Yingjie Yu [a,*], Chongtian Huang [b], Liansheng Sui [c], Kemao Qian [d], Anand Asundi [b]

[a] Department of Precision Mechanical Engineering, Shanghai University, Shanghai 200072, China
[b] School of Mechanical and Aerospace Engineering, Nanyang Technological University 639798, Singapore
[c] School of Computer Science and Engineering, Xi'an University of Technology, Shaanxi Province 710048, China
[d] School of Computer Engineering, Nanyang Technological University 639798, Singapore

ARTICLE INFO

Keywords:
Fringe pattern
Denoising
Deep learning

ABSTRACT

In this paper, deep learning as a novel algorithm is proposed to reduce the noise of the fringe patterns. Usually, the training samples are acquired through experimental acquisition, but these data can be easily obtained by simulations in the proposed algorithm. Thus, the time cost used for the whole training process is greatly reduced. The performance of the proposed algorithm has been demonstrated through the analysis on the simulated and real fringe patterns. It is obvious that the proposed algorithm has a faster calculation speed compared with existing denoising algorithm, and recovers the fringe patterns with high quality. Most importantly, the proposed algorithm may provide a solution to other denoising problems in the field of optics, such as hologram and speckle denoising.

1. Introduction

Interferometry as a non-contact high-precision measurement technology can recover the phase distribution from the fringe pattern. Many fringe demodulation methods have been proposed to obtain high-precision phase distribution, such as the phase-shifting interferometry [1] and the windowed Fourier transform algorithm [2]. However, the noise can cause severe distortion in the estimated phase distribution of the measured object, and denoising is a necessary pre-processing step to analyze the fringe patterns. Wang et al. [3] proposed a coherence enhancing diffusion method for fringe denoising. Qian [4,5] proposed the windowed Fourier filter algorithm (WFF). Fu and Zhang [6] proposed an image decomposition method to reduce the noise of fringe pattern. Uzanet et al. [7] proposed the nonlocal means filter for speckle denoising of digital holography. Although these existing denoising methods that achieve satisfactory denoising results, these methods will spend much time to process a large number noisy of fringe patterns. Thus, developing an intelligent method to quickly process a large number of fringe patterns with satisfied denoising results, will play an important role in the field of optical measurement based on fringe patterns.

With the remarkable improvement of computing power, deep learning [8] as a powerful algorithm allows the multi-layer network to learn characteristics of data. Many practical problems have been solved by deep learning including image super-resolution [9], video recognition [10] and speech recognition [11]. Deep learning as a general tool has also penetrated into the field of optics such as ghost imaging [12], phase recovery and holographic image reconstruction [13], classification of data for holographic memory [14], identification and classification of objects hidden behind scattering media [15] and object estimation from unseen raw intensity images [16].

To obtain high-precision phase measurement results, deep learning is proposed to reduce the noise of fringe pattern in this paper, where the deep convolutional neural network (DCNN) model is trained by using a series of noisy fringe patterns and the corresponding noiseless fringe patterns, namely ground truth. After the DCNN has been trained, the fringe pattern with noise is used as the input data of the DCNN model, and the fringe pattern without noise can be predicted in the DCNN output. The training data and their related ground truths are simulated, which is easier and faster than experimental acquisition. The advantage of the proposed method is that DCNN model has better denoising performance than the compared algorithm in the boundary of the fringe pattern. Most importantly, the proposed DCNN model has a faster denoising speed compared with the existing algorithm, which is verified by the analysis on simulations and experiments.

2. Principle of the proposed method

Mathematically, an interference fringe image can be expressed as:

$$I(x,y) = I_0(x,y) + \gamma(x,y)\cos[\phi(x,y)] + I_n(x,y) \quad (1)$$

Where (x,y) is the spatial coordinate, $I_0(x,y)$ is the background intensity, $\gamma(x,y)$ and $\phi(x,y)$ are the amplitude and desired phase distribution, respectively, $I_n(x,y)$ is an additive noise. It is difficult to demodulate

* Corresponding author.
E-mail address: SHU_YYJ@126.com (Y. Yu).

https://doi.org/10.1016/j.optcom.2018.12.058
Received 17 October 2018; Received in revised form 11 December 2018; Accepted 16 December 2018
Available online 21 December 2018

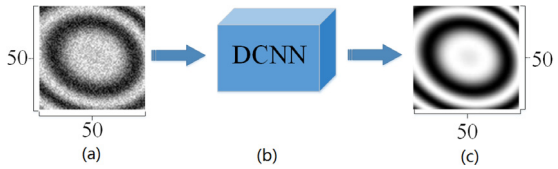

Fig. 1. Schematic diagram of the deep learning algorithm for the fringe denoising: (a) the fringe pattern with noise; (b) the proposed DCNN model; (c) the predicted result by the proposed DCNN.

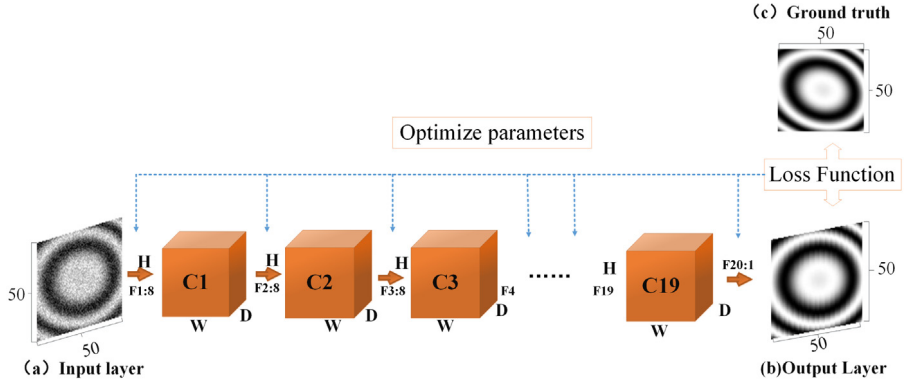

Fig. 2. The structure of the DCNN model: C1 to C19 represents the feature map of each layer, respectively; W, H and D represents the length, width and thickness of the feature map of each layer, respectively; The kernel of each convolutional layer is represented by F (shown as F1 to F20).

the fringe if the fringe pattern contains high additive noise [17]. For a single noisy fringe pattern, the deep learning algorithm is proposed to reduce the additive noise $I_n(x, y)$, with the schematic diagram shown in Fig. 1.

In Fig. 1, deep convolution neural network (DCNN) model in the deep learning algorithm is used for denoising, which is an end-to-end calculation. Fig. 1(a) is a fringe pattern with noise, which is calculated as the input layer by the DCNN model to obtain the noiseless fringe (shown in Fig. 1(c)). Fig. 1(b) is the DCNN model we proposed, as illustrated in Fig. 2.

The DCNN model contains 20 convolutional layers as shown in Fig. 2, the fully-connected layer and pooling layer are not used in here. In the network structure, the kernel size of F1 to F19 is fixed to 3×3×1 pixels, the size of F20 is fixed to 1×1×1 pixels. The stride of the kernel is fixed to 1 pixel in the entire network structure. For the number of the kernel, F1 to F5 is 8, F6 to F8 is 32, F9 to F11 is 64, F12 to F14 is 32, F15 to F19 is 8 and F20 is 1. The padding is fixed to 1 pixel for each layer of convolution. By the above parameter setting, the length and width of the feature map of each layer have a fixed size of 50×50 pixels. In our DCNN model, to make our DCNN model have more learning performance to solve nonlinear problems, the output of each convolutional layer is nonlinearly mapped by an activation function with rectified linear units (ReLU) [18].

Fig. 2(a) as the input layer is composed of the fringe pattern with noise. The image has a size of 50×50 pixels and its gray level is represented by 8 bits. The input fringe pattern is filtered by the convolutional layer with 8 kernels of size 3×3×1 pixels, the stride of the kernel is 1 pixel, where the input fringe pattern is padding with 1 pixel. In Fig. 2(C1), the first feature map is obtained by feature extraction of the kernel and nonlinear mapping of ReLU. According to the above principle of the feature extraction, the same principle is used for each convolution layer. Finally, the output layer of the DCNN model is obtained as shown in Fig. 2(b). The ground truths in Fig. 2(C) are the corresponding fringe pattern without noise with the same size. Then the DCNN model is trained to optimize parameters by Adam [19] (Adaptive Moment Estimation) algorithm, which ultimately finds the best weight parameter to minimize the loss function between the predicted result of DCNN and the corresponding ground truth. The loss function is as follows:

$$Loss(x, y) = \frac{1}{p}\sum \left| x_j - y_j \right| \tag{2}$$

where x_j is the output of the DCNN, y_j is the ground truth, p is the number of the element.

To generate the training set to train the DCNN, the input fringe pattern with noise and the corresponding ground truths are generated with Eq. (1). To simulate the unknown values of the amplitude and background intensity, the background intensity is randomly taken in the range of 90 to 130, and the amplitude is randomly taken in the range of 80 to 110. It is well known that the Zernike polynomials [20] describe the classical aberrations of an optical system, and the Zernike polynomials have the same form as the types of aberrations often observed in optical tests [21]. Therefore, the wavefront characteristics are represented by Zernike polynomials fitting as follows:

$$\phi(x, y) = \sum_{n=1}^{N} a_n z_n \left(x_k, y_k \right) \tag{3}$$

where $\phi(x, y)$ is the wavefront and a_n represents the coefficients of the Zernike polynomials, $z_n\left(x_k, y_k\right)$ is the Zernike terms and n is the number of terms. Fig. 3 shows the typical monochrome fringe pattern, which is represented by the first 8 terms of the Zernike polynomials, respectively.

By randomly taking the value of the aberration coefficient a_n, various wavefronts are generated by the first 21 terms ($n = 21$) of the Zernike polynomials with Eq. (3). After setting the range of the above parameters, the fringe pattern is simulated based on Eq. (1). Three kinds of Gaussian noise with ($\mu = 0, \sigma = 2$), ($\mu = 0, \sigma = 5$) and ($\mu = 0, \sigma = 8$) are added to the fringe pattern as the training samples, respectively , where the symbol μ represents the mean and σ represents the standard deviation.

Finally, 80,000 pairs of noisy fringe patterns and corresponding ground truths are generated, and input into the DCNN for training. The DCNN is implemented using Python language and the framework of Pytorch on a PC with Intel®Core™i7-7820X CPU@3.60GHz×13, the GeForce GTX 1080 (NVIDIA) is used to accelerate the computation. The different learning rates for the DCNN model are used, which can be adjusted automatically after each epoch. First, the fixed learning rate is set to a large value of 0.001. The model is trained for 7 epochs

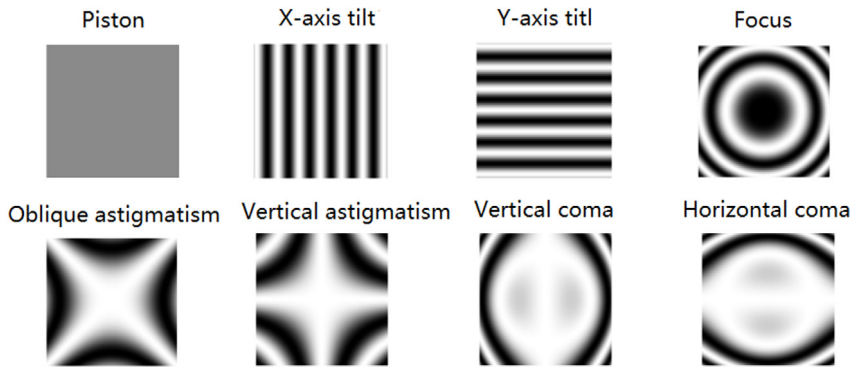

Fig. 3. Typical monochrome fringe pattern.

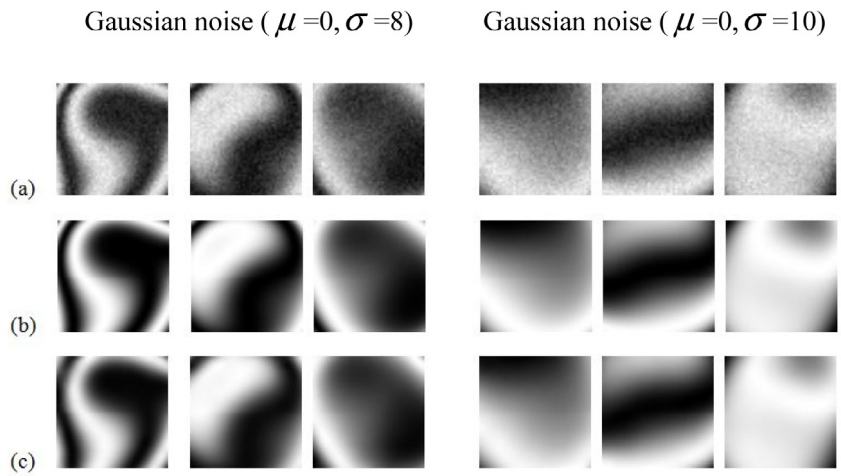

Fig. 4. Test result by the proposed DCNN: (a) the simulated fringe pattern with noise; (b) the ground truth and (c) the predicted result by the proposed DCNN.

and the learning rate is set to 6×10^{-4},then the learning rate of 13 epochs and 19 epochs is set to 3.6×10^{-4}, 2.16×10^{-4}, respectively. Finally, the learning rate of 25 epochs, 31 epochs, 37 epochs, 43 epochs, 49 epochs and 55 epochs is set to the small values of 1.296×10^{-4}, 0.7776×10^{-4}, 0.4666×10^{-4}, 0.2799×10^{-4},0.168×10^{-4} and 0.1008×10^{-4},respectively. After 60 epochs, our DCNN model has been trained and the entire training process takes approximately 12 h.

3. Testing and analysis

To evaluate the performance of DCNN for fringe pattern denoising, we use the data that is not included in the training set to test the trained DCNN. We use the Eq. (1) to generate six sets of fringe pattern with Gaussian noise, three sets of fringe patterns has Gaussian noise with ($\mu = 0, \sigma = 8$), the other three sets of fringe patterns has Gaussian noise with ($\mu = 0, \sigma = 10$). The sizes of these fringe patterns are 50×50 pixels. The values of the background intensity and amplitude are set to 145 and 75, respectively. According to Eq. (3), the first 10 terms of the Zernike polynomials are used to represent the wavefront. The fringe pattern simulated by the above parameter values is shown in Fig. 4.

In Fig. 4, six sets of fringe patterns with different noises are predicted by the DCNN. The first row (a) is calculated as the input layer by the trained DCNN, the second row (b) shows the ground truth corresponding the first row (a), and the predicted result is shown in the third row (c). The visual observation shows that noise is removed by our DCNN from the noisy fringe pattern successfully.

Another simulated fringe pattern with the size of 215×215 pixels is also used to evaluate the denoising performance of the DCNN, which has Gaussian noise with ($\mu = 0, \sigma = 7$) as depicted in Fig. 5(a). The wavefront is also calculated by the first 10 terms of the Zernike polynomials. In addition, the values of the background intensity and amplitude are 140, 90, respectively. Fig. 5(c) is the predicted result by our trained DCNN, the whole prediction process only takes 2.1413 s. It can be seen from

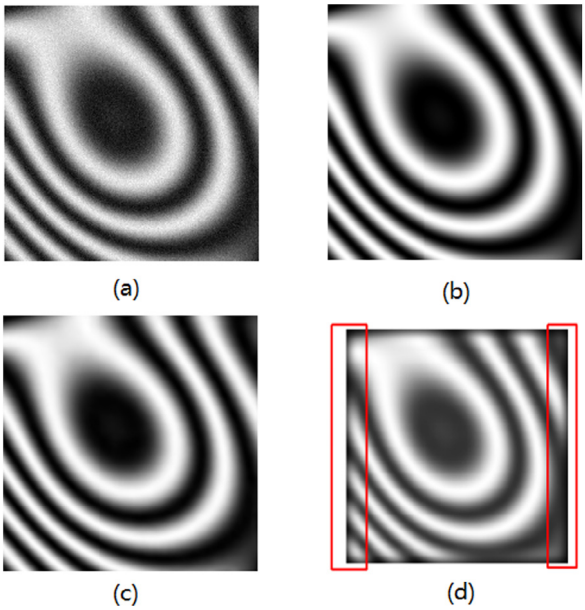

Fig. 5. The result: (a) the fringe pattern with noise, (b) the ground truth, (c) the denoising result by the DCNN and (d) the denoising result by WFF.

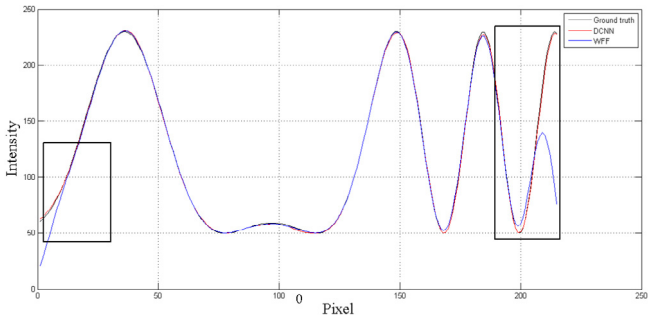

Fig. 6. The comparison of the algorithm in the 100th column from Fig. 5(b), (c) and (d).

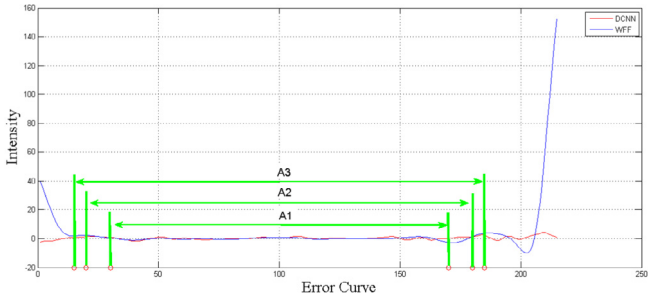

Fig. 7. Plotting error curves of the 100th column of Fig. 5(c) and (d).

Fig. 5(c) that the denoising effect is obvious, which is smooth compared with Fig. 5(a).

The denoising performance of our DCNN is further demonstrated by compared the DCNN result in Fig. 5(c) with the windowed Fourier filter algorithm (WFF) in Fig. 5(d). It is obvious that the DNCC performance better around image boundaries, as highlighted by red rectangular boxes in Fig. 5(d). In WFF, zero-padding is used by default, which affects the filtering results in the boundary area. The DCNN provides a useful solution if information around the boundaries is of importance.

Fig. 6 shows a detailed comparison of the pixels in the 100th column from Fig. 5(b), (c) and (d), respectively. We can clearly see that the DCNN is closer to the ground truth. The WFF is obviously different from the ground truth in the boundary area, which has been marked in the black boxes as shown in Fig. 6.

In order to see the contrast in details, Fig. 7 shows error curves of the 100th column of Fig. 5(c) and (d), which is obtained by subtracting the ground truth. As it can be seen obviously, the red curve represents the error of DCNN, which is closer to 0 and has better denoising performance from the overall perspective. To compare the error distribution of DCNN and WFF, the mean square error (MSE) of Fig. 7(A1), (A2) and (A3) is shown in Table 1, respectively.

As shown with the MSE comparison above, although denoising performance of WFF is better than DCNN in the middle area, the results

Table 1
MSE comparison.

Range	DCNN	WFF
A1	0.5061	0.3825
A2	0.6187	0.7547
A3	0.7650	1.1635

of both methods do not have the obvious difference. However, the DCNN has achieved more significant denoising performance than WFF for the whole fringe pattern, especially for the boundary of the fringe pattern. More notably, the noisy fringe pattern can be quickly denoised by our well-trained DCNN in the test phase, and a large number of noisy fringe patterns can be automatically denoised without any adjustment of parameters.

4. Experiments

As it is described above, the denoising performance of the DCNN has been analyzed by the simulated fringe pattern. In our experiment, to demonstrate the success of the DCNN denoising method in the real fringe pattern, six sets of the fringe patterns are collected from the interferometer experimental platform as shown in Fig. 8.

In Fig. 8, the size of the real fringes with serious noises in the first row(a) is 150×150 pixels, which are collected from the Zygo and 4D interferometer. The predicted results are shown in the second row (b). Through visual observation, the noisy fringe pattern is estimated by our DCNN to obtain a smooth fringe pattern. In Fig. 9, another real fringe pattern with the size of 170×110 pixels is further verified by the DCNN, which is collected from the Zygo interferometer.

It is shown that the fringe pattern of Fig. 9(b) is very smooth and the noise is almost non-existent. We also use the WFF to perform fringe pattern denoising as shown in Fig. 9(c). Fig. 9(d) shows the comparison result of DCNN and WFF in the 50th column from (b) and (c), respectively. Both methods improve denoising performance compared with the real fringe pattern, but the error decreases rapidly in the boundary of the fringe pattern with the proposed DCNN. It can be further concluded that our DCNN has better denoising performance for the whole fringe pattern. In addition, the denoising process only takes 2.1407 s for one fringe pattern, which reduces much time compared with the existing algorithm.

5. Conclusion

In this paper, the denoising method for the fringe patterns is proposed based on the powerful deep learning. The obvious advantage of the proposed DCNN is that a large number of noisy fringe patterns and their ground truths can be easily simulated with the related formula, which greatly decreases the cost of applications. Compared with the existing denoising algorithm, the proposed method has a faster calculation speed. The experimental result has been verified with the real fringe

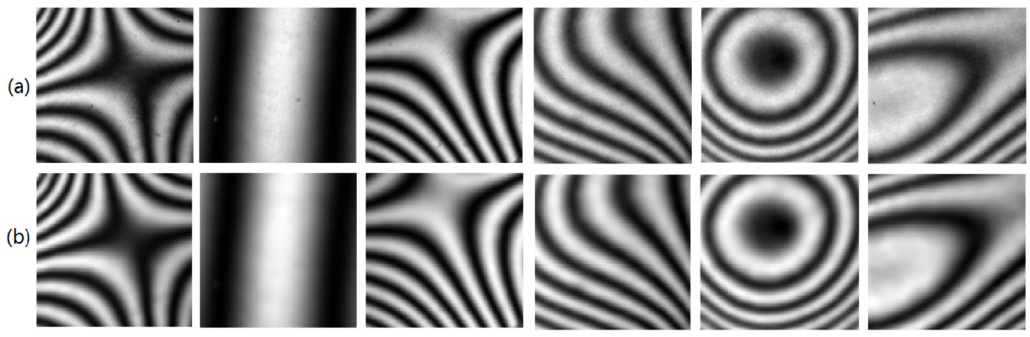

Fig. 8. Experimental results: (a) the real fringes; (b) the denoising results by our DCNN.

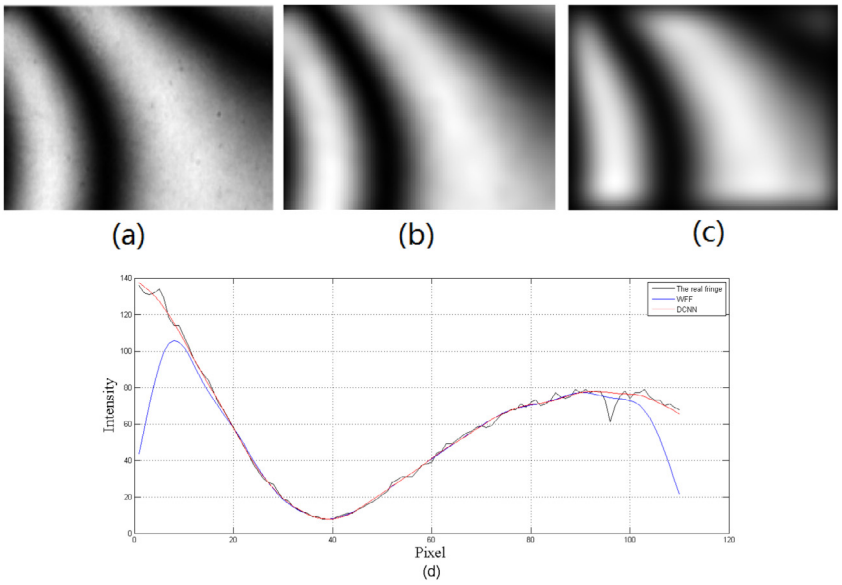

Fig. 9. Experimental results: (a) the real fringe pattern; (b) the denoising result by our DCNN; (c) the denoising result by the WFF; (d) the pixel variation curve of the 50th column from (a), (b) and (c).

pattern, where the denoising result with high quality can be obtained. Furthermore, the proposed method has stable performance and there is no need to adjust any parameters.

Acknowledgment

This work was supported by the National Natural Science Foundation of China (NSFC) (No. 51775326).

References

[1] K. Hibino, Y. Kim, S. Lee, Y. Kondo, N. Sugita, M. Mitsuishi, Simultaneous measurement of surface shape and absolute optical thickness of a glass plate by wavelength tuning phase-shifting interferometry, Opt. Rev. 19 (2012) 247–253.
[2] K. Qian, H. Wang, W. Gao, Windowed fourier transforms for fringe pattern analysis: theoretical analyses, Appl. Opt. 47 (2008) 5408–5419.
[3] H. Wang, K. Qian, W. Gao, F. Lin, H. Seah, Fringe pattern denoising using coherence- -enhancing diffusion, Opt. Lett. 34 (2009) 1141–1143.
[4] K. Qian, Windowed fourier transform for fringe pattern analysis, Appl. Opt. 43 (2004) 2695–2702.
[5] K. Qian, Two-dimensional windowed fourier transform for fringe pattern analysis: principles, applications, and implementations, Opt. Lasers Eng. 45 (2007) 304–317.
[6] S. Fu, C. Zhang, Fringe pattern denoising via image decomposition, Opt. Lett. 37 (2012) 422–424.
[7] A. Uzan, Y. Rivenson, A. Stern, Speckle denoising in digital holography by nonlocal means filtering, Appl. Opt. 52 (2013) 195–200.
[8] Y. LeCun, Y. Bengio, G. Hinton, Deep learning, Nature 521 (2015) 436–444.
[9] C. Dong, C. Loy, K. He, X. Tang, Learning a deep convolutional network for image super–resolution, in: 13th European Conference on Computer Vision, ECCV 2014, Zurich, Switzerland, 2014, pp. 184–199.
[10] X. Zhu, Y. Xiong, J. Dai, L. Yuan, Y. Wei, Deep feature flow for video recognition, in: Proceedings–30th IEEE Conference on Computer Vision and Pattern Recognition, CVPR 2017, Honolulu, HI, United states, 2017, pp. 4141–4150.
[11] A. Graves, A. r. Mohamed, G. Hinton, Speech recognition with deep recurrent neural network, in: 38th IEEE International Conference on Acoustics, Speech, and Signal Processing, ICASSP 2013, Vancouver, BC, Canada, 2013, 6645–6649.
[12] M. Lyu, W. Wang, H. Wang, H. Wang, G. Li, N. Chen, G. Situ, Deep-learning-based ghost imaging, Sci. Rep. 7 (2017) 17865.
[13] Y. Rivenson, Y. Zhang, H. Gunaydin, D. Teng, A. Ozcan, Phase recovery and holographic image reconstruction using deep learning in neural networks, Light Sci. Appl. 7 (2018) 17141.
[14] T. Shimobaba, N. Kuwata, M. Homma, T. Takahashi, Y. Nagahama, M. Sano, S. Hasegawa, R. Hirayama, T. Kakue, A. Shiraki, N. Takada, T. Ito, Convolutional neural network-based data page classification for holographic memory, Appl. Opt. 56 (2017) 7327–7330.
[15] G. Satat, M. Tancik, O. Gupta, B. Heshmat, R. Raskar, Object classification through scattering media with deep learning on time resolved measurement, Opt. Express 25 (2017) 17466–17479.
[16] A. Sinha, J. Lee, S. Li, G. Barbastathis, Lensless computational imaging through deep learning, Optica 4 (2017) 1117–1125.
[17] F. Cuevasa, J. Sossa-Azuela, M. Servin, A parametric method applied to phase recovery from a fringe pattern based on a genetic algorithm, Opt. Commun. 203 (2002) 213–223.
[18] V. Nair, G. Hinton, Rectified linear units improve restricted boltzmann machines, in: 27th International Conference on Machine Learning, ICML 2010, Haifa, Israel, 2010, pp. 807–814.
[19] D. Kingma, J. Ba, Adam: A method for stochastic optimization, in: Proceedings of the 3rd International Conference on Learning Representations, ICLR 2015, 2015.
[20] R.J. Noll, Zernike polynomials and atmospheric turbulence, J. Opt. Soc. Am. 66 (1976) 207–211.
[21] J. Wyant, K. Creath, Basic wavefront aberration theory for optical metrology, Appl. Opt. Opt. Eng. 11 (1992) 28–39.